NeuroImage 206 (2020) 116325

Contents lists available at ScienceDirect

NeuroImage

journal homepage: www.elsevier.com/locate/neuroimage

Prediction-error signals to violated expectations about person identity and head orientation are doubly-dissociated across dorsal and ventral visual stream regions

Jonathan E. Robinson [a,b,c,*], Will Woods [d], Sumie Leung [d], Jordy Kaufman [d], Michael Breakspear [c,e], Andrew W. Young [f], Patrick J. Johnston [a,b,c]

[a] School of Psychology and Counselling, Queensland University of Technology, Victoria Park Road, Kelvin Grove, QLD, 4059, Australia
[b] Institute of Health and Biomedical Innovation, 60 Musk Avenue, Kelvin Grove, QLD, 4059, Australia
[c] QIMR Berghofer Medical Research Institute, 300 Herston Road, Herston, QLD, 4006, Australia
[d] Brain & Psychological Sciences Research Centre, Swinburne University of Technology, Burwood Road, Hawthorn, VIC, 3123, Australia
[e] School of Psychology, University of Newcastle, University Drive, Callaghan, NSW, 2308, Australia
[f] Department of Psychology, University of York, Heslington, YO10 5DD, United Kingdom

ARTICLE INFO

Keywords:
Face processing
MEG source localisation
Prediction-error
Visual processing hierarchy
Predictive coding

ABSTRACT

Predictive coding theories of perception highlight the importance of constantly updated internal models of the world to predict future sensory inputs. Importantly, such theories suggest that prediction-error signalling should be specific to the violation of predictions concerning distinct attributes of the same stimulus. To interrogate this as yet untested prediction, we focused on two different aspects of face perception (identity and orientation) and investigated whether cortical regions which process particular stimulus attributes also signal prediction violations with respect to those same stimulus attributes. We employed a paradigm using sequential trajectories of images to create perceptual expectations about face orientation and identity, and then parametrically violated each attribute. Using MEG data, we identified double dissociations of expectancy violations in the dorsal and ventral visual streams, such that the right fusiform gyrus showed greater prediction-error signals to identity violations than to orientation violations, whereas the left angular gyrus showed the converse pattern of results. Our results suggest that perceptual prediction-error signalling is directly linked to regions associated with the processing of different stimulus properties.

Predictive coding formulations of perception consistently emphasise the importance of hierarchical prediction-error signalling mechanisms that allow the brain to test internally generated models of the world against actual sensory input (Dayan et al., 1995; Friston and Kiebel, 2009; Hohwy, 2013). A largely untested aspect of such models is whether prediction-errors that signal violations of a particular stimulus attribute arise at the same level of the processing hierarchy as that at which the attribute is resolved (Friston, 2005). Alternatively, error signalling could reflect a more pervasive phenomenon encompassing multiple brain regions.

The visual system provides an excellent test-bed for disambiguating these possibilities, as it is well established that distinct visual processing streams subserve particular stimulus attributes (Milner and Goodale, 1998; Mishkin et al., 1983). Mishkin et al. (1983) first described two cortical channels of visual information processing: object recognition processes occur in regions along the ventral surface of the brain; whilst the processing of visuo-spatial information occurs in brain regions along the dorsal surface. This division has been particularly well reflected in the study of face perception (Andrews and Ewbank, 2004; Haxby et al., 2000; Kanwisher et al., 1997). The ventrally located fusiform gyrus (FG) has been identified as a cortical region involved in the recognition of relatively fixed properties of faces, such as face identity (Grill-Spector et al., 2004). By comparison, time varying aspects of the face, such as head motion, head orientation, and facial expression are commonly attributed to more dorsally located regions, such as the middle temporal, superior temporal and angular gyri (Allison et al., 2000; Baseler et al., 2012; Carlin et al., 2011; O'Toole et al., 2002).

In a previous study (Johnston et al., 2017), we identified

* Corresponding author. School of Philosophy, History and International Studies, Monash University, Wellington Road, Clayton, VIC, 3800, Australia.
E-mail address: jonathan.robinson@monash.edu (J.E. Robinson).

https://doi.org/10.1016/j.neuroimage.2019.116325
Received 26 April 2019; Received in revised form 22 October 2019; Accepted 29 October 2019
Available online 1 November 2019

early-latency expectancy violation responses (~110–210 ms) to unexpected head and body orientations. These responses were localised to relatively dorsal visual areas of middle temporal, superior temporal and angular gyri. Indeed, we also identified comparable early-latency responses for violations of visual expectation in relation to face identity (Johnston et al., 2016), typically considered to involve the ventral stream. These prior studies suggest that responses in this time window may reflect similar processes relating to the reconciliation of top-down predictions and bottom-up sensory encoding. Our previous studies (Johnston et al., 2016; Robinson et al., 2018) also report a consistent mid-latency response to violated prediction in both identity and orientation violations. This mid-latency response was proposed to be involved in higher level perceptual processing and reorientation of attention.

However, despite this suggestion of a consistent signalling process to violated expectation across these attributes, it remains to be seen whether the corresponding prediction-errors arise from those regions where the core stimulus processing occurs. It is also unclear whether different types of violations share a similar temporal profile. The present magnetoencephalography (MEG) study aims to reconcile these issues. Crucially, we exploit the fact that the face is a source of multiple signals (Bruce and Young, 2012; Young, 2018) to investigate whether expectancy violations can be differentially localised to their respective perceptual streams. In a widely used neural model (Haxby et al., 2000) the core system for face perception involves two distinct processing pathways: a ventral pathway targeted at the fusiform gyrus for the analysis of relatively invariant aspects of faces (such as face identity); and a more dorsal pathway, toward posterior STS, involved in the analysis of changeable aspects of faces (such as orientation). Importantly face stimuli are also well known to elicit strong, early-latency event-related responses (Eimer, 2011), that should maximise the detection of responses to expectancy violations. By contrasting the localisation of prediction-errors to violated expectations involving face identity, with those associated with head orientation, we can test whether prediction-errors are relatively circumscribed (i.e. involving more ventral regions for violations of expected identity and more dorsal regions for violations of expected orientation) or propagated throughout the core visual system.

Our investigation combines a novel source localisation and time course analysis to identify potential double dissociations to violated expectations associated with the facial identity trajectory or the orientation trajectory in a sequence of face images. To achieve this we adapted the contextual trajectory paradigm described in our previous work (Johnston et al., 2017; Robinson et al., 2018) to create and subsequently violate expectations relating to each of these stimulus attributes. If prediction-error signalling is relatively circumscribed to the brain regions involved in processing particular attributes, we predicted that there should be a double dissociation in error signalling during the early to mid response latency. Specifically, we predicted that: 1) violated expectations about head orientation should result in responses localised to relatively dorsal, but not ventral stream regions; and 2) violated expectations about face identity should result in responses that localise to ventral but not to more dorsal regions.

1. Materials and methods

1.1. Participants

Data were acquired from twenty-two (11 female) participants, all of whom self-reported right handedness. The age of participants ranged between 19 and 48 years ($M = 26.05$ years, $SD = 7.35$ years).

1.2. Stimuli

Images of five upright exemplar faces were captured using a Professional 3D Graphics Rendering software (Poser 11). Exemplar images were captured on a black background, at 2-degree head orientation increments (in virtual space) ranging between −26° and 34°, with 0° corresponding to a directly forward-facing stimulus. Virtually rendered faces were used in order to maintain precise control over the angle of orientation, whilst also maintaining eye gaze, light source, head roll and pitch, and facial expression. A constraint on maximal head orientation was defined such that all face parts (eyes, lips, etc) were at least partially visible in every image. All rendered exemplar images used monochromatic male subjects (see Fig. 1). Each image was enclosed in a 300×300 pixel frame (72 ppi) using Adobe Photoshop (CC, 2015). Additionally, using MATLAB (v.2016b, MathWorks), all exemplars were matched for mean luminance (RGB pixel Value $117 \pm 1\%$) across each image set and resized to give them a similar amount of black background ($\pm 2\%$) (i.e. the area of black background not filled by the image subject). Duplicates of each image set were created with red dots added to each image in a random position on the face of the image subject. These images with superimposed red dots were used for the vigilance task described in the procedure below.

Stimuli were presented using PsychoPy (v1.85.1) (Peirce, 2007, 2009) on a computer (Dell) activated by the experimenter and projected (Panasonic PT – D5100 projector) using a mirror periscope in the wall of the magnetically shielded room that surrounded the MEG. The periscope back projected the experiment onto a nonferrous projector screen (1.5×1 m) placed ~1 m from the participant, such that the stimuli filled ~2 degrees of the visual angle. A response box was also given to the participants so they could respond to red dot vigilance trials. All participants performed accurately (>80% accuracy) on the vigilance task during the experiment and so none were excluded on this basis.

1.3. Procedure

The present study employed an adaptation of the contextual trajectory paradigm (Johnston et al., 2017) to test for a possible dissociation between expectancy violations relating to face identity and those relating to head orientation trajectories. The original paradigm used a sequence of five images that transitioned through a range of positions (orientations or compass winds) to create a contextually bound expectation about the object's trajectory. In this previous experiment a given trial finished with either a predicted or unpredicted (violating) final stimulus transition, based on the implied trajectory of the preceding sequence. Crucially, the present study used sequences of five images sampled from seven possible stimulus positions (1–7) and was carefully designed to involve clockwise and counter-clockwise orientation sequences that could then be collapsed across during analysis. These orientation sequences were created so that the final two stimuli were matched across both predictable (1-2-3-4-5) and unpredictable (7-6-5-4-5) trial instances, with comparable matching of the final two stimuli for the opposite trajectory direction (predictable: 7-6-5-4-3; unpredictable: 1-2-3-4-3).

As with the contextual trajectory paradigm used in Johnston et al. (2017), then, the design of the present experiment ensured a match in the final transition across orientation conditions, such that every 'predictable' trial had a final stimulus transition that was physically identical to an 'unpredictable' trial. Moreover, our adaptation of the design also ensured that no trial sequence contained any identical stimulus repeat. The present experiment used multiple rotation increments (8° and 10°) for the transitions in head orientation, thereby preventing the repeat of an identical stimulus within a given trial. Data were then collapsed across clockwise and counter-clockwise sequences during the analysis.

Participants viewed sequences of five successive images of heads in each trial. The final image in relation to the preceding sequence varied to form the different conditions: The fifth and final image in each sequence either confirmed or violated the expectation about the image subject's head Orientation or Identity (see Fig. 1).

In order to create identical final transitions across Violations (sequences with unpredictable final images) and Non-violations (sequences with predictable final images) in both Identity and Orientation, it was important to include identity sequences that did not elicit surprise but

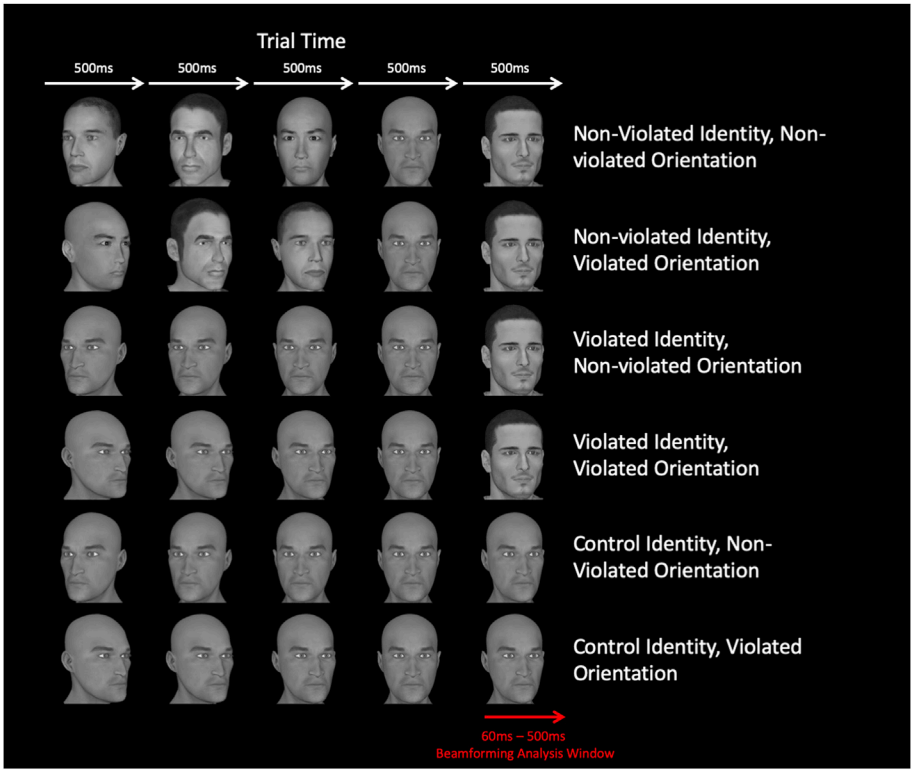

Fig. 1. An example sequence for each of the six experimental conditions is shown in each row. In notational form (N - Non-violated, V = Violated, I = Identity, O = Orientation), each pair of sequence rows (from top to bottom) represents different Identity conditions: Non-violated Identity conditions in rows 1 (NINO) and 2 (NIVO), Violated Identity in rows 3 (VINO) and 4 (VIVO), and the Control Identity conditions in rows 5 (CINO) and 6 (CIVO). Alternate sequences (from top to bottom) thus represents the two possible Orientation conditions: Non-violated Orientation (NINO, VINO, CINO) and Violated Orientation (NIVO, VIVO, CIVO). Note that each trial sequence across the four main conditions (NINO, NIVO, VINO, VIVO) is matched to the final transition, and the two baseline conditions are also matched across the final transition.

had identically matched final transitions for both Violated Identity and Non-violated Identity conditions. For this reason, the study used continuously changing Non-violated Identity conditions (see top rows of Fig. 1), where a different facial identity was presented in every step of the sequence, such that no expectation about identity could be established across the trial sequence. By comparison, the Violated Identity trials presented a consistent identity for the first four stimuli of the sequence, with a different identity in the final transition that violated the accumulated expectation (middle rows of Fig. 1). This trial design, coupled with the adapted orientation sequences used previously, allowed us to create parametric sets of trial sequences that ended with an identical final transition for Identity or Orientation violations. These trial sequences were used to create the two factors of interest: Expectation Type (Identity; Orientation) and Predictability (Violated; Non-violated). Two types of trial sequence consisted of Non-violated Identities in which orientation was either Non-violated (Non-violated Identity Non-violated Orientation - NINO) or Violated (Non-violated Identity Violated Orientation - NIVO) in the final transition. By comparison two types of trial sequences contained Violated identities in the final transition, with either a Non-violated orientation (Violated Identity Non-violated Orientation - VINO) or Violated orientation (Violated Identity Violated Orientation - VIVO). Because of the consistently matched final transition over each of these conditions, any differences in the event related fields (ERF) across these conditions must have reflected the preceding context rather than any low-level stimulus differences in the onset of the final stimulus (because there were none).

Additionally, we ensured that not all sequences containing repeated identities were Violated identity trials. If this were the case, a Violated Identity could be assumed following the onset of the second image of its sequence and the trial outcome might become predictable. Therefore, as can be seen in Fig. 1 (bottom rows), two additional conditions were used as Control Identity conditions which maintained a consistent identity within each trial sequence, but which used either a Non-violated orientation (CINO) or Violated orientation (CIVO) in the final transition. These conditions replicated previous contextual trajectory paradigms (Johnston et al., 2017; Robinson et al., 2018) where an unchanging (predictable) identity was presented across all transitions of a trial and only orientation was manipulated.

Each identity used in the study appeared in all sequence positions, and all conditions equally often, matched across the four main experimental conditions (NINO, NIVO, VINO, VIVO) and separately across both of the control conditions (CINO, CIVO). All trajectory sequences used a penultimate image at a fixed transition point (4°) that enabled a match of stimuli in Orientation conditions. This transition point was intentionally offset from the centre (0°) to prevent any disruption due to participants responding to known effects of being looked at directly (Jenkins et al., 2006). Half of all trials involved a Non-violated Orientation sequence and half involved a Violated Orientation sequence.

Stimuli were presented for 500 ms each, creating a total trial length (five stimuli) of 2.5 s, with a 500 ms fixation cross presentation between each trial. Eighty trials were presented randomly for each condition in the experiment, constituting a total of 480 experimental trials. In order to ensure vigilance throughout the experiment, an additional 60 “red dot trials” were added, distributed randomly throughout the experiment (~11% of the total trials). These trials featured one of the stimuli with a superimposed red dot at a random point in the sequence, with participants being instructed to respond via a button press when they saw the red dot image, using the button box provided. These red dot vigilance monitoring trials were excluded from the analysis. This gave the experiment a total of 540 trials, lasting approximately 27 min.

1.4. MEG and MRI acquisition parameters

Data were acquired using the Elekta TRIUX MEG (306 channel; 102 magnetometers and 204 gradiometers) at the Brain and Psychological Sciences Centre (BPsyC), SUT. The data were recorded at a rate of 1000 Hz, with an online high-pass filter of 0.1 Hz and an online low-pass filter of 300 Hz. Fiduciary electrodes were attached to both mastoids, and the left, right, and centre of the forehead in order to monitor the participants’ motion in the scanner. Electrodes were also attached above and below the right eye to monitor blinks, to the right wrist to monitor cardiac rhythm, and to the right elbow for grounding. The registration of the

scalp in 3D space was achieved using a Polhemus 3D pen, which marked the position of each fiduciary electrode, the nasion, and both the left and right tragus. The pen was then used to draw an outline of the entire head shape in the 3D tracking software. The position of fiduciary electrodes was then recorded throughout the scan to ensure the head position could be tracked in relation to the sensors in the scan.

This information and the 3D plot of the head shape were then used for coregistration with anatomical Magnetic Resonance Imaging (MRI) data, to enable anatomical inference in source-space analysis. Each individual's digitised head shape was coregistered with their individual MRI data using surface matching (Kozinska et al., 2001). The high resolution T1-weighted structural MRI volume was acquired with a Siemens Tim Trio 3T MRI scanner, using a 12-channel head coil. The spatial resolution of the scan was $1.0 \times 1.0 \times 1.0$ mm, reconstructed to 1 mm isotropic voxels; a TR of 1900 ms; a TE of 2520 ms; a TI of 900 ms; a flip-angle of 9°; and field-of-view of 256 mm on a voxel matrix of 256 by 176. The total scan time for the T1 structural MRI was approximately 8 min. The structural volume of each participant was segmented using FreeSurfer (v6.0.0) (Fischl et al., 2002) and a nonlinear transformation was applied to calculate equivalent coordinates in the MNI 152 standard brain, using ANTS (Avants et al., 2009). A regular 5 mm × 5 mm x 5 mm grid was defined on the MNI brain, and the inverse transformation applied to the grid points for each individual, resulting in a one-to-one anatomical correspondence for each grid point across the group.

1.5. MEG pre-processing

For each participant, MEG data were initially segmented into 3000 ms windows around the final stimulus of each experimental trial, extending −2500 ms prior to final stimulus onset, to encompass the entire trial, and 500 ms after the final stimulus, in order to encompass the post-stimulus response. These data segments were then individually inspected by the research team, using a bespoke (Python v2.7.14) tool to visualize data variance by trial and sensors. Those sensors or trials highlighted for containing particularly high variance were excluded from further analysis. The data from all remaining magnetometers and gradiometers were filtered using a Butterworth filter with a high-pass of 1 Hz and low-pass of 40 Hz, with a slope −24 dB/octave.

1.6. Statistical analyses

Consistent with our previous MEG studies (Simpson et al., 2015) a two-stage analysis strategy was applied, with the addition of an orthogonal post-hoc data driven analysis (in stage two) in order to address the double dissociation hypothesis. The first stage of the analysis identified any regions where there were significant differences between Violated and Non-violated conditions separately for Identity and Orientation conditions. It is important to note that in a particular contrast (e.g. Violated identity vs. Non-violated Identity) the identification of significant voxels does not in itself indicate significant differences between violations in this contrast and the other contrast, and furthermore that this analysis does not identify when in time a difference is present. Therefore, in a second stage we investigated whether, within time windows where effects were present, an orthogonal effect relating specifically to the hypothesis was expressed. For this reason, a second stage of analysis was required to identify time windows for further consideration, but also crucially to test for a double dissociation between these conditions across dorsal and ventral stream regions.

In the first stage of the analysis, two spatial beamforming analyses were used to localise cortical regions. The Identity comparison used compound conditions of all Non-violated Identity (NINO, NIVO) compared to all Violated Identity conditions (VINO, VIVO). The Orientation comparison combined all conditions containing Non-violated Orientations (NINO, VINO, CINO) and compared them to all conditions containing Violated Orientations (NIVO, VIVO, CIVO). In stage 2, the virtual electrode (VE) time series, at each cortical location identified in stage 1, were analysed to establish *when* in time the relevant comparison showed statistically significant differences at these cortical locations. We then tested whether those regions in the dorsal and ventral stream showed any double dissociation of Expectation Type (Identity or Orientation) over this time period.

1.7. Stage one: source localisation of violated predictions in identity and orientation

To identify brain regions that respond to Identity or Orientation violations, a beamforming analysis was performed. This first step of the analysis was to separately localise activity associated with differences in the face Identity conditions (Non-violated Identity vs. Violated Identity) or differences in the head Orientation conditions (Non-violated Orientation vs. Violated Orientation). This was achieved using two contrasts, as described above. Within each comparison, the difference in the total power of the average evoked response for each condition was calculated across a time window, where any trial related signal should have occurred, for every grid point location within each individual's 3D coregistered anatomical MRI image. The time window was considered as 60 ms–500 ms, where 0 ms was the time of onset of the fifth image in each sequence. Performing the analysis across this time window was necessary to gain a robust estimate of covariance, precluding any temporal analysis in this stage of the analysis. In addition, a leave-one-out jack-knife procedure was used to estimate the standard error of this difference at each location.

The beamformer generated VE time series in source space for each epoch of data in the conditions being compared. These timeseries were dc corrected (using the period −200 ms–0 ms) and orientated to maximise the difference in evoked power between comparison conditions, in a similar manner to the Maximum Contrast Minimum Variance Beamformer introduced by Chen et al. (2006). These VEs invert signals from the sensors to model the time series at each location in a volumetric grid over the brain (as described in the supplementary Methods). To identify statistically significant local maxima at the group level (corrected $p < .05$ two tailed), we adopted a non-parametric permutation (1,000 times) procedure using maximum statistics to control for the FWE (Nichols and Holmes, 2002). The analysis only considered grid points included in a grey matter mask generated with the Harvard-Oxford cortical structural atlas parcellation (Desikan et al., 2006; Frazier et al., 2005; Goldstein et al., 2007; Makris et al., 2006) as implemented in FSL (FMRIB, Software Library v5.0). More specific details on calculation of the Beamformer metric are available in Supplementary Materials (Supplementary Methods).

1.8. Stage two: time window selection within the VE evoked timeseries

Overview. The beamformer metric provided a dipole orientation that maximises the difference between comparison conditions across the period of evoked signal (60–500 ms post stimulus). However, this first stage of the analysis was agnostic with respect to when in time any differences occur, optimal orientation for individual conditions, and the dipole direction. Therefore, Stage Two of the analysis was required to identify the latencies of any differences in the data and to clarify whether these differences formed a double dissociation with the alternative set of conditions.

The time series of local maxima identified in each of the two beamforming analyses were estimated for each condition (1. Non-violated Identity; 2. Violated Identity; 3. Non-violated Orientation; 4. Violated Orientation) by passing sensory data for each trial in each condition back through the beamformer weights at the specified brain location, in order to estimate a 3D time series referred to as a virtual electrode (VE). As in stage one this 3D timeseries was then oriented to maximise the differences of the relevant main effect comparisons at each location. Each trial time series was therefore expressed as a one-dimensional vector that could then be dealt with in a similar way to normally epoched data.

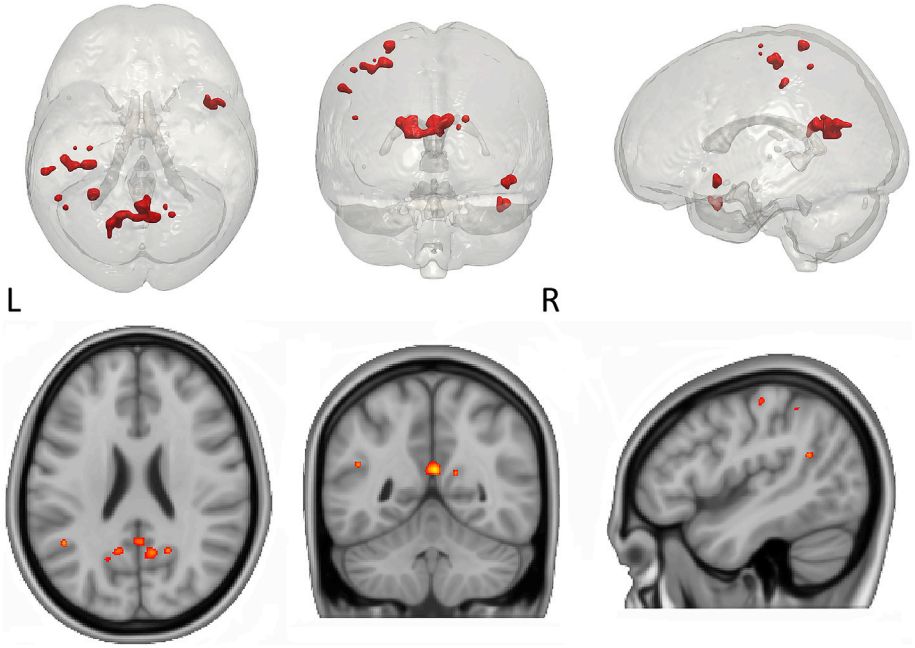

Fig. 2. The bottom panel shows key selected slices of a *t*-values heat map from the Orientation localisation (NINO–CINO–VINO vs. NIVO-CIVO-VIVO) displayed on the MNI 152 standard brain. The top panel shows a 3-D rendering of the same data on a transparant MNI brain, with significant voxels displayed in red. 3-D meshes were constructed using ITK-SNAP (v.3.6.0) (Yushkevich et al., 2006), thresholded to $p < .05$ ($t = -6.451$) based on a non-parametric null distribution created by permuting the condition labels to produce a threshold for each localisation.

Within each participant, the absolute values for the mean timeseries (ERF) of each condition were needed, to allow statistical comparisons across participants. This was necessary to make participants' VEs comparable, as the VE could be oriented according to either end of the dipole for a given participant. First, comparisons were performed for window selection, to identify the time windows in which there were significant differences in Predictability (Non-Violated vs. Violated). Comparisons were performed only within the maxima associated with the specific beamformer localisation for Orientation (Non-violated Orientation vs. Violated Orientation) and for Identity (Non-violated Identity vs. Identity). Then, in the average amplitude section of the VE analysis a summary statistic, across the identified window, was extracted from the timeseries of each condition. In an orthogonal comparison VEs from either comparison identified in the Dorsal stream could then be tested for a double dissociation of Expectation Type (Orientation vs. Identity) against VEs identified in Ventral Stream and vice versa.

Window Selection. Instead of performing statistics across a pre-specified time window and analysing the total power differences, to avoid biasing the VE timeseries analysis, windows of importance were defined by performing a *t*-test at each time point (0–500 ms) of the time series. Accordingly, two sets of cluster permutation t-tests were performed (see Supplementary Fig. 5). One set of tests was performed at the associated VEs locations comparing Orientation conditions (NINO, VINO, CINO < NIVO, VIVO, CIVO), whilst a second set of tests was performed on Identity VEs comparing Identity conditions (NINO, NIVO < VINO, VIVO). Each set was compared to a permuted null distribution over Orientation VEs and identity VEs separately. Selection of the VE subset for this analysis was based on the proximity of VEs to surrounding maxima in the same contrast, preferencing on the basis of voxel intensity (i.e. for VEs less than 20 mm^3 from any other VE maxima, the VE with the voxel with the highest *t*-value was selected). To correct for multiple comparisons in these t-tests, the analysis used a temporal clustering correction. Non-parametric cluster-wise inference was performed with an initial common height threshold, $t(21) = 1.721$, $p < .05$, using a summed cluster value method. Correction for multiple comparison was performed using a sign-flip permutation (10,000 times) method (Nichols and Holmes, 2002). Cluster-wise correction considered the time series VEs separately, using a corrected threshold of $p < .05$. VEs containing significant clusters therefore demonstrated differences between Violated and Non-violated conditions for their particular Expectation Type. Only VEs from this subset situated in either the Ventral or Dorsal Stream were included in the final analysis.

Average Amplitude Analysis. The average amplitude for these ventral and dorsal stream VEs was extracted across the identified time windows. In a post-hoc data driven comparison, using the differences identified in the previous step, we investigated our initial hypothesis; that is, we attempted to identify whether any double-dissociations between Region Location (Dorsal x Ventral) and Expectation Types (Orientation x Identity). Given that predictability conditions have been tested for within Expectation Type and comparisons must be normalised across different sources, we computed the log-ratio of average amplitudes across Predictability conditions (Violated or Non-violated) for each Expectation Type (Orientation or Identity). To test our main hypothesis, these values were then analysed using a repeated-measures ANOVA to consider pairs of VEs with the factors of Region Location (Ventral vs. Dorsal) and Type of Expectation (Orientation vs. Identity). Crucially, any significant interaction of these factors in any time window would identify a double-dissociation between the Type of Expectation and Region. Here we used a Bonferroni correction to account for the number of ANOVAs performed ($\alpha = .0125$).

2. Results

2.1. Stage one: source localisation of violated predictions in identity and orientation

This stage of the analysis considered the whole brain using a metric derived from a beamforming analysis (see supplementary Methods). This approach enabled the separate localisation of brain regions activated for identity violation and orientation violation. To provide sufficient power, the analysis of each stimulus attribute compared all Non-violated and Violated conditions that were fully matched for the final transitions across this comparison. As such, the Orientation localisations involved all six conditions (NINO; VINO; CINO; NIVO; VIVO; CIVO), whereas the Identity localisations only considered four conditions (NINO; NIVO; VINO; VIVO) to ensure an identical final transition across Non-violated and Violated Identity conditions.

Orientation localisations and Identity localisations demonstrated notably different significant voxels. The Orientation localisation highlighted significant differences in activity between Non-violated Orientation and Violated Orientation conditions (Fig. 2) in dorsally located

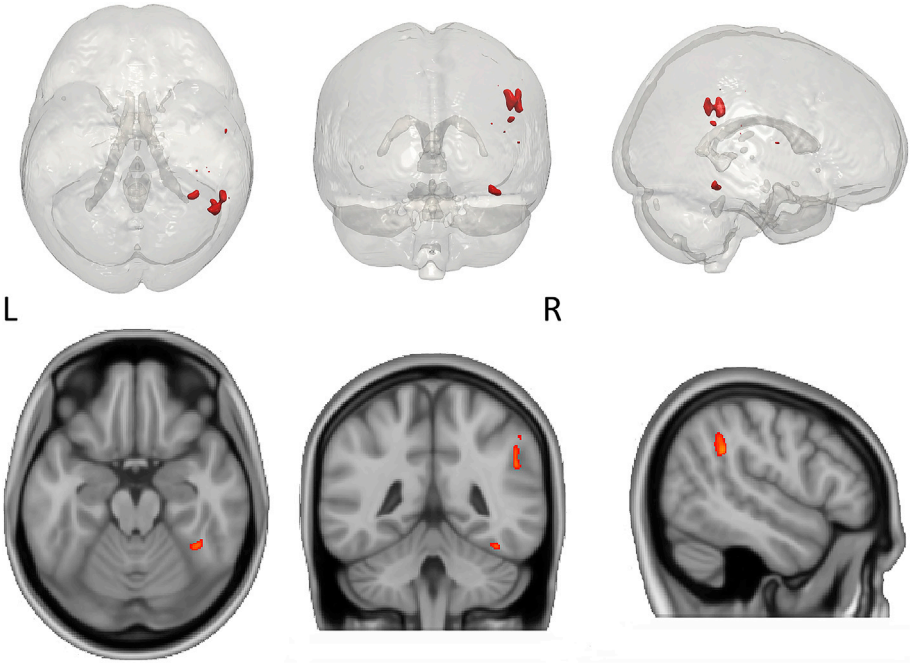

Fig. 3. The bottom panel shows key selected slices of a *t*-values heatmap from the Identity localisation (NINO–NIVO vs. VINO-VIVO) displayed on the MNI 152 standard brain. The top panel shows a 3-D rendering of the same data on a transparant MNI brain with significant voxels displayed in red. 3-D meshes were constructed using ITK-SNAP (v.3.6.0) (Yushkevich et al., 2006). This was thresholded to $p < .05$ ($t = -6.648$) based on a non-parametric null distribution created by permuting the condition labels to produce a threshold for each localisation.

brain regions such as the left angular gyrus ($t = -8.555$ $p < .05$ corrected). By comparison, the Identity localisation identified differences between Non-violated Identity and Violated Identity conditions (Fig. 3) in ventrally located regions in the right temporal occipital fusiform ($t = -7.871$, $p < .05$ corrected). The *t*-values generated by the beamformer metric for the Identity and Orientation conditions identified a number of other peak local maxima that met the threshold for significance (see Table 1). Each significant local maximum was considered for subsequent VE analysis.

2.2. Stage two: time windows selected within the VE evoked timeseries

Window Selection. A subset of the local maxima identified in each Stage One comparison (Table 1) were selected for further analysis. In each localisation, for all local maxima less than 20 mm^3 from one another, the voxel with the highest *t*-intensity was selected. Of the 15 regions identified in the Orientation localisation (see Supplementary Fig. 1 & Supplementary Fig. 2), a subset of 10 were selected for further analysis. From the seven locations identified in the Identity localisation (see Supplementary Fig. 3 & Supplementary Fig. 4), a subset of five were included in the subsequent VEs analysis. The VE analysis extracted an estimated time course for each trial at each of the selected voxel locations (Table 2). The timeseries from the four types of compound conditions were extracted: 1. NINO, CINO, VINO; 2. NIVO, CIVO, VIVO; 3. NINO, NIVO; 4. VINO, VIVO. In each case, absolute values of the mean timeseries were generated, for all selected VEs, within every participant.

Two temporal clustering analyses were performed, to identify significant differences in the Non-violated and Violated conditions in the Orientation and Identity comparisons. This revealed a number of clusters that exceeded the significance threshold value in both comparisons (see Table 3). Significant temporal clusters were found for each comparison within both early and mid-latency time-windows.

The Orientation comparison revealed three regions, each containing one significant temporal cluster (Fig. 4) that exceeded a threshold value of 45.14 ($p < .05$ corrected): in the left precuneus between 238 and 310 ms ($t = 54.47$, $p < .05$ corrected); left angular gyrus between 146 and 237 ms ($t = 56.88$, $p < .05$ corrected); left postcentral gyrus between 194 and 238 ms ($t = 50.42$, $p < .05$ corrected). Each of these clusters showed significantly higher response amplitudes to the final stimulus in Violated

Table 1
Significant local maxima identified by the beamformer metric *t*-test for each experimental localisation.

Beamformer Metric Localisation	Regions	Intensity (*t*)	x	y	z
Orientation	Posterior cingulate cortex	−9.969	3	−51	19
	Left precuneus	−9.514	−18	−62	19
	Left postcentral gyrus	−9.212	−26	−41	67
	Right precuneus	−8.555	9	−58	22
	Left angular gyrus	−8.555	−45	−52	23
	Right precuneus	−8.303	19	−57	22
	Right temporal pole	−7.950	49	12	−31
	Right temporal pole	−7.899	47	13	−17
	Left supramarginal gyrus	−7.899	−56	−30	43
	Left postcentral gyrus	−7.849	−43	−22	56
	Right temporal pole	−7.395	53	13	−15
	Left supramarginal gyrus	−7.142	−64	−28	31
	Right supramarginal gyrus	−7.142	57	−31	38
	Left hMT/V5	−6.739	−43	−68	−2
	Right superior frontal gyrus	−6.739	21	15	49
Identity	Right angular gyrus	−9.464	46	−52	33
	Right angular gyrus	−8.257	51	−43	30
	Right temporal occipital fusiform gyrus	−7.871	36	−47	−19
	Right supramarginal gyrus	−6.953	41	−27	44
	Right central opercular cortex	−6.857	55	−6	10
	Right parietal operculum	−6.857	37	−30	20
	Right planum temporal	−6.760	45	−30	15

Note. Voxels are considered significant based on a non-parametric null distribution created by permuting the condition labels to produce a threshold for each comparison (alpha = .05). Intensity values are based on *t*-tests of leave-one-out distributions for each condition. Locations are based on MNI 152 (x,y,z) coordinates. Values are interpolated from a 5 mm × 5 mm grid to the MNI 152 standardised 1 mm × 1 mm voxel T1 brain image.

Table 2
VE selection for timepoint by timepoint *t*-test analysis.

Beamformer Metric Localisation	Index	Locations	x	y	z	Intensity (*t*)
Orientation	1	Left hMT/V5	−43	−68	−2	−6.739
	2	Left precuneus	−18	−62	19	−9.514
	3	Left angular gyrus	−45	−52	23	−8.555
	4	posterior cingulate	3	−51	19	−9.969
	5	Left postcentral gyrus	−26	−41	67	−9.212
	6	Right Supramarginal gyrus	57	−31	38	−7.142
	7	Left Supramarginal gyrus	−56	−30	43	−7.899
	8	Left Postcentral gyrus	−43	−22	56	−7.849
	9	Right temporal Ppole	49	12	−31	−7.950
	10	Right superior frontal gyrus	21	15	49	−6.739
Identity	1	Right angular gyrus	46	−52	33	−9.464
	2	Right temporal occipital fusiform	36	−47	−19	−7.871
	3	Right parietal operculum	37	−30	20	−6.857
	4	Right supramarginal gyrus	41	−27	44	−6.953
	5	Right central opercular cortex	55	−6	10	−6.857

Note. This VE subset was reordered according to their y coordinates in MNI space. Indices are used in subsequent t-tests to denote VEs.

Orientation sequences as compared to Non-violated Orientation sequences.

The Identity comparison highlighted five regions with significant clusters, each containing one significant temporal cluster (Fig. 5) that exceeded the permuted threshold value of 62.48 ($p < .05$ corrected): in the right angular gyrus between 166 and 447 ms ($t = 344.44$, $p < .001$ corrected); in the FG between 175 and 463 ms ($t = 272.72$, $p < .01$ corrected); in the right parietal operculum between 219 and 412 ms ($t = 301$, $p < .0001$ corrected); right supramarginal gyrus between 279 and 370 ms ($t = 69.731$, $p < .05$ corrected); right central opercular cortex between 254 and 404 ms ($t = 237.89$, $p < .01$ corrected). Each of these demonstrated a larger response to Violated as compared to Non-violated Identity Conditions that was not present for the orientation conditions.

Average Amplitude Analysis. To test directly for the presence of double dissociations between neural responses to violations of Identity and Orientation in ventral and dorsal stream regions, we performed four ANOVAs involving regions located in the dorsal vs. ventral stream. These regions were selected post-hoc, based on the presence of a significant time window response in the previous analysis. Each ANOVA considered factors of Expectation Type (Orientation vs. Identity) and Region Location (Dorsal vs. Ventral); an interaction between these factors would therefore be indicative of a double dissociation. The ANOVAs used the log-ratio of the time window averages across predictability (Violated or Non-violated) for each Expectation Type. For this analysis, the only significant VE within the ventral stream was in the FG, whilst the left angular gyrus, left postcentral gyrus, right angular gyrus, and right supramarginal gyrus were all considered to be within the dorsal stream.

The ANOVA involving the FG and left angular gyrus demonstrated an interaction between Region Location and Expectation type ($F_{(1,21)} = 16.35$, $p = .001$, $\eta_p^2 = 0.438$) but no main effects. Similarly the comparison of the FG and left postcentral gyrus highlighted an interaction ($F_{(1,21)} = 21.72$, $p < .001$, $\eta_p^2 = 0.508$) but no main effects. Boxplots highlight the crossover interaction between Orientation and Identity conditions in comparisons of these sites (see Fig. 6). Here, the FG shows a greater response to Identity Violations, whilst Orientation Violations elicit a greater response in the dorsal stream.

In contrast, the comparison of the FG and right angular gyrus demonstrated only a main effect of Expectation Type ($F_{(1,21)} = 22.93$, $p < .001$, $\eta_p^2 = 0.522$). For the comparison of FG and the supramarginal gyrus the Expectation Type main effect ($F_{(1,21)} = 5.49$, $p = .029$, $\eta_p^2 = 0.207$) did not reach statistical significance with Bonferroni correction ($\alpha = 0.0125$). At these sites, then, both ventral and dorsal stream VEs show a larger response to Identity Violations than to Orientation Violations (see Fig. 7).

3. Discussion

Our study explored the relative involvement of dorsal and ventral visual areas in early-latency prediction-error responses. By comparing activity related to violations of orientation with activity related to identity, we identified and dissociated predictive processes between dorsal and ventral visual regions. Specifically, MEG Beamformer contrasts revealed distinct cortical regions that showed activation to violations of expected head Orientation (including regions of the dorsal and medial parieto-temporal cortices, and the left temporal pole) in contrast to violations with respect to face Identity (including the fusiform gyrus, and regions of right dorsal parieto-temporal and opercular cortices).

The beamformer metric used for whole brain analysis needed a sufficiently long window to establish stable estimates of covariance; in this case we used 60–500 ms post onset of the final stimulus in each sequence, which encompassed the majority of the evoked power in the signal. We then calculated VE timeseries based on the regions identified by the beamformer, and used a temporal clustering permutation method to establish the time windows during which the timeseries to Non-violated and Violated expectation trials showed significantly different amplitudes. This revealed a subset of regions for each of the two comparisons (involving violations of expected Orientation or Identity) that showed significant temporally constrained differences in signal amplitude. For Orientation: the left precuneus, left angular gyrus, left postcentral gyrus; for Identity: right angular gyrus, right temporal occipital fusiform, right

Table 3
List of temporal clusters for VE comparison based on timepoint by timepoint *t*-test (violation vs. non-violation) in each condition.

Analysis of Variance Results	Region	x	y	z	Window Latency (ms)	Cluster *t*-value	Cluster *p*-Value
Orientation Time windows	Left precuneus	−18	−62	−19	238–310	54.57	.023*
	Left angular gyrus	−45	−52	23	146–237	56.88	.019*
	Left postcentral gyrus	−43	−22	56	194–237	50.42	.031*
Identity Time windows	Right angular gyrus	46	−52	33	166–447	344.44	.0001****
	Right temporal occipital fusiform	36	−47	−19	175–463	272.72	.002**
	Right parietal operculum	37	−30	20	219–412	301	.0008***
	Right supramarginal gyrus	41	−27	44	279–370	69.73	.04*
	Right central opercular cortex	55	−6	10	254–404	237.89	.006**

Note. Values considered significant follow a correction using sign flip permutations (10,000 times). Asterisks signify the corrected p-value thresholds, p < .05 (*), p < .01 (**), p < .001 (***), p .0001 (****). Locations are presented in MNI 152 Coordinates (x y z).

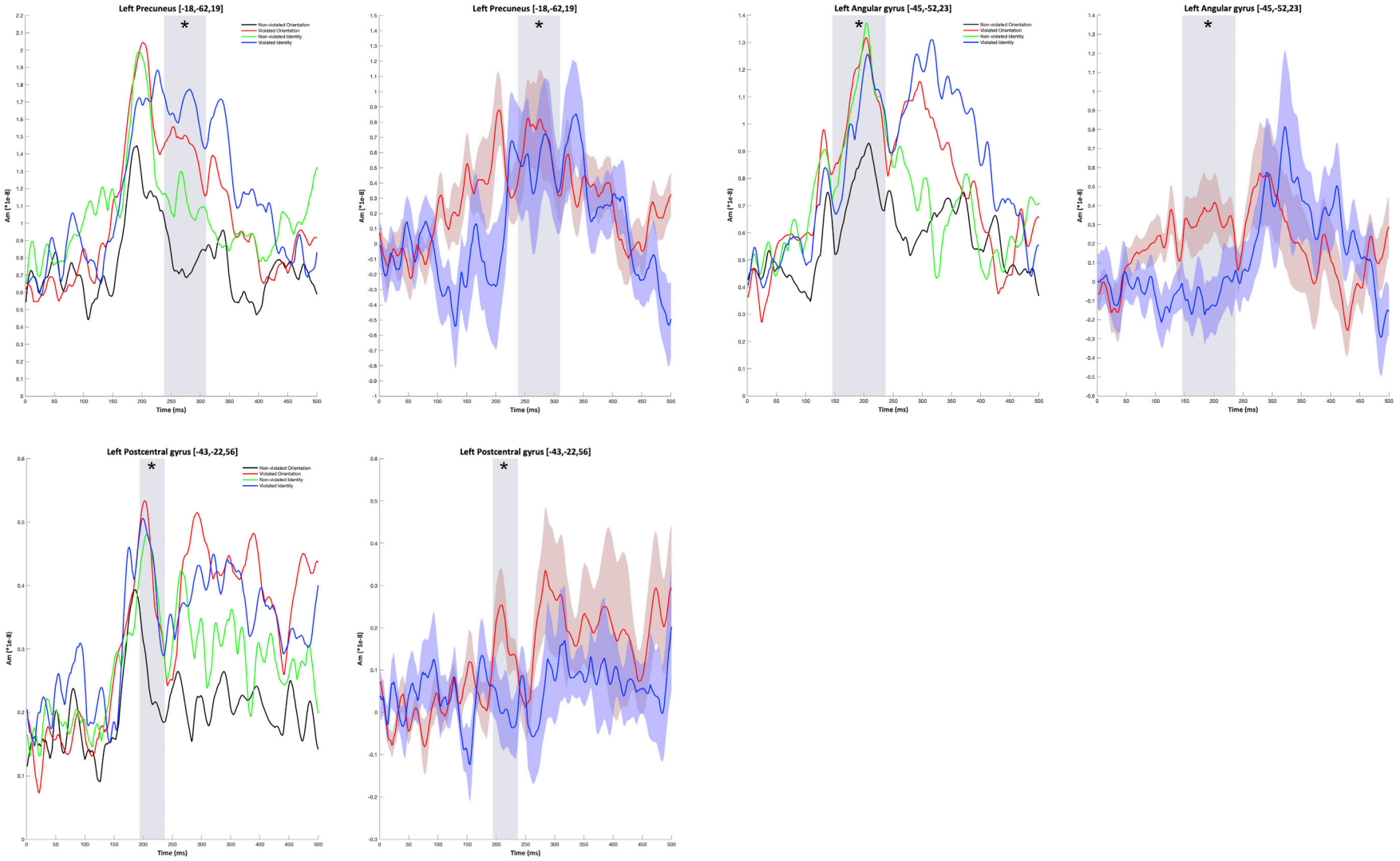

Fig. 4. Selected VE time series from the Orientation window selection. On the left timeseries are presented for Non-violated Orientation (in black), Violated Orientation (in red), Non-violated Identity (in green), and Violated Identity conditions (in blue). On the right timeseries of the difference waveforms are presented for Orientation (in red) and Identity (in blue). Time series are baselined to the first 50 ms after onset of the final stimulus in each sequence. Shaded grey sections represent significant time windows for VE. Shading around timeseries on the right represent ± 1 standard error for the respective time series.

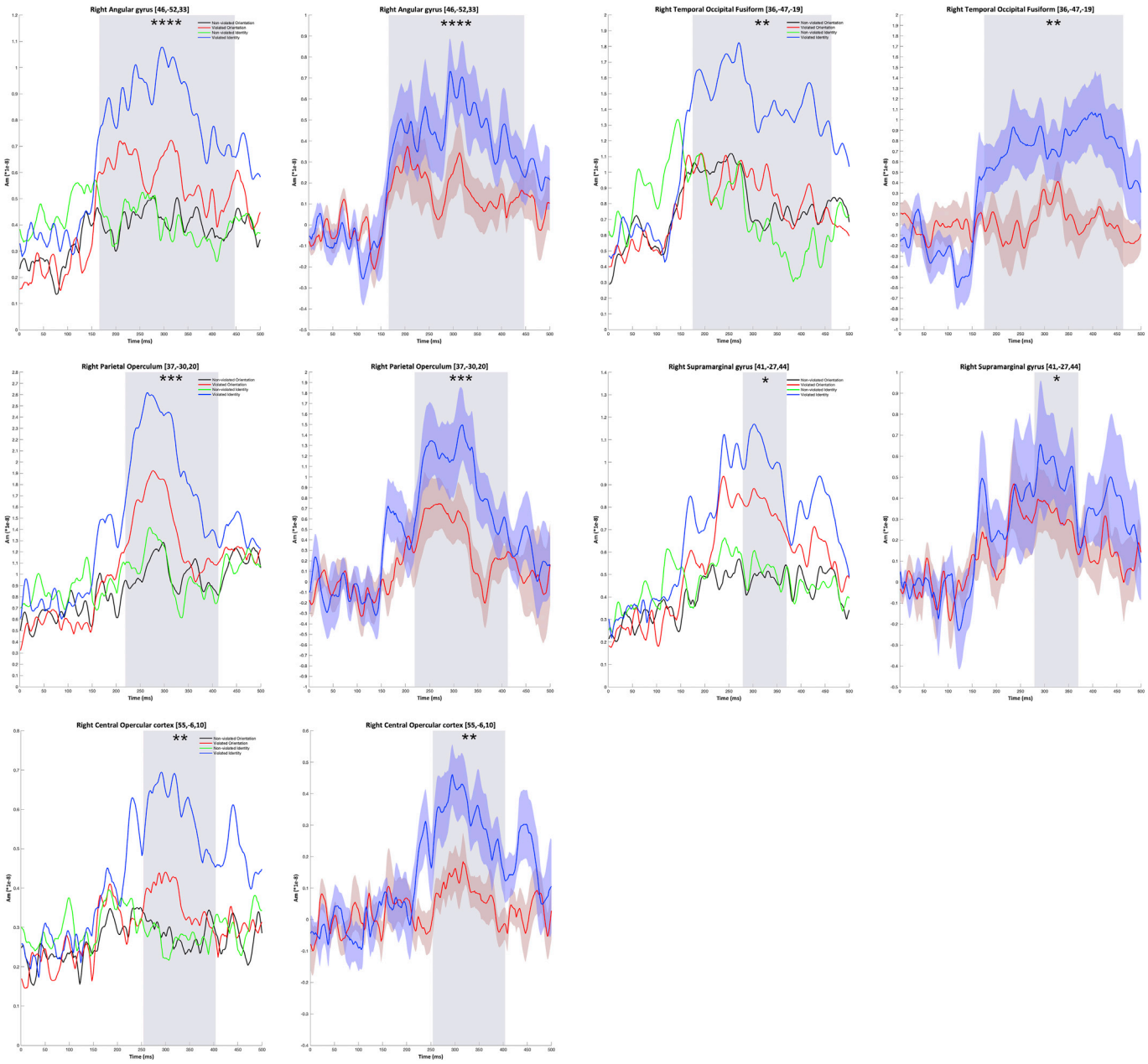

Fig. 5. Selected VE time series from the Identity window selection. On the left timeseries are presented for Non-violated Orientation (in black), Violated Orientation (in red), Non-violated Identity (in green), and Violated Identity conditions (in blue). On the right timeseries of the difference waveforms are presented for Orientation (in red) and Identity (in blue). Time series are baselined to the first 50 ms after onset of the final stimulus in each sequence. Shaded grey sections represent significant time windows for VE. Shading around timeseries on the right represent ± 1 standard error for the respective time series.

parietal operculum, right supramarginal gyrus, and right central opercular cortex.

The outcome that other VEs identified by the beamformer analysis did not show significant differences between Non-violated and Violated conditions, in Orientation or Identity *across specific time-windows*, may reflect one of two main possibilities. Either insufficient power to detect such differences, or that any consistent differences in evoked power between the conditions were not time-locked to a specific latency window. For the respective VEs, we used main effects contrasts of Orientation and Identity conditions separately to determine whether there was evidence of temporally constrained expectation violation signals. Based on this, we extracted averaged signal amplitudes for each time window for all four types of trial (Non-violated Orientation, Violated Orientation, Non-violated Identity, Violated Identity). We then compared log-ratios (Violated/Non-violated) of amplitudes using four ANOVAs to create the critical test for a double dissociation of interaction effects involving Region Location (Dorsal vs. Ventral) and Expectation Type (Identity vs. Orientation. This revealed a pattern of findings consistent with evidence of early to mid-latency double-dissociations between dorsal and ventral cortical regions. Specifically, the right fusiform gyrus (175–463 ms) was compared to the left angular gyrus (146–237 ms) and the left postcentral gyrus (194–237). There was greater activation to violated expectations relating to head orientation than to face identity in the left angular gyrus and the left postcentral gyrus. Indeed, the opposite was also true, with a larger violation response for Identity as compared to orientation in the right fusiform gyrus. The comparison of the right fusiform gyrus to each of these regions thus demonstrated a clear double dissociation of function between these dorsal stream regions and the ventral region (fusiform). In

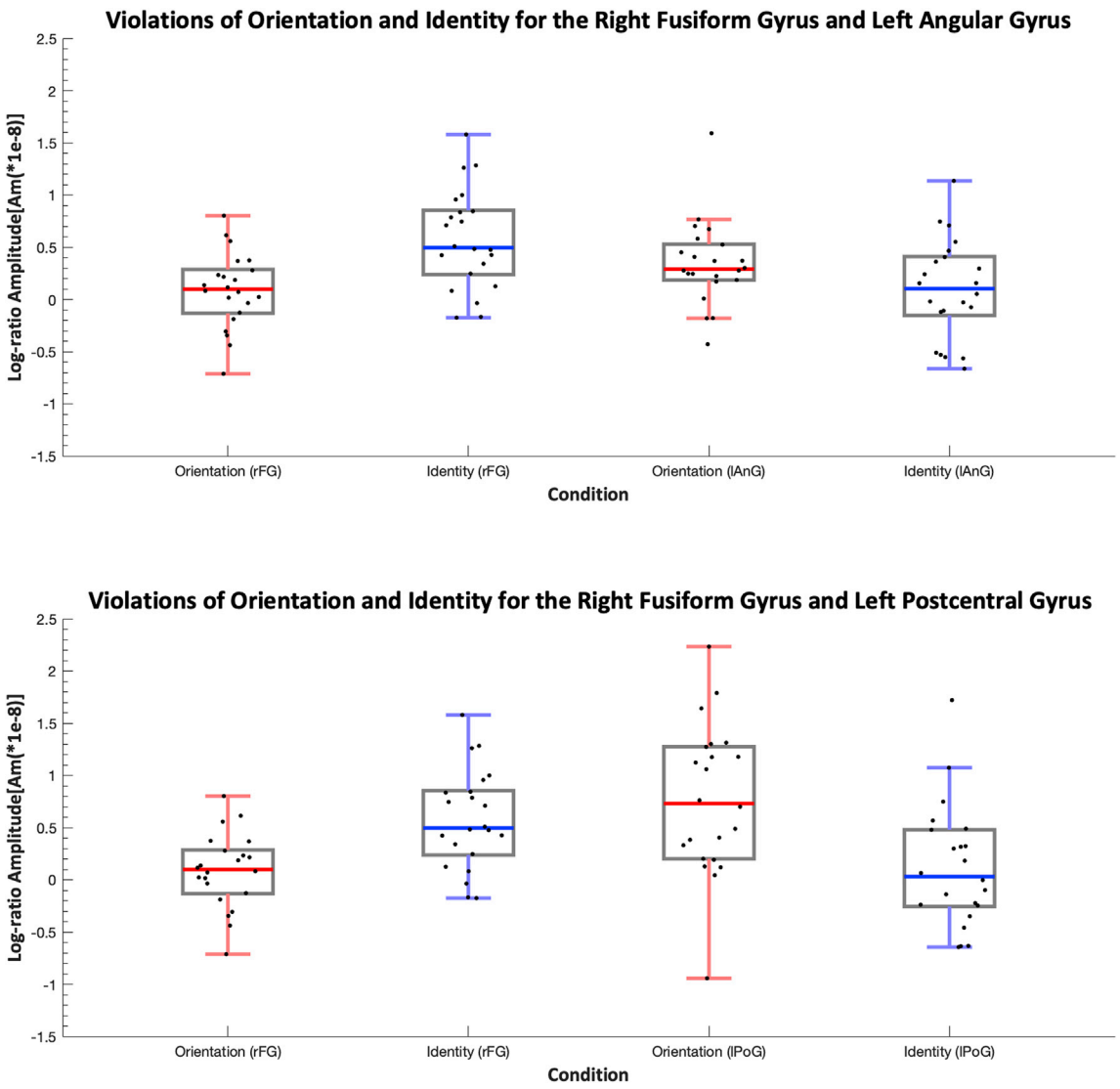

Fig. 6. Difference box plots of Identity (in blue) and Orientation (in red) conditions for the log-ratio (Violated/Non-violated) of average amplitude across selected windows (see Table 3). The plots show pairs of regions from the ventral and dorsal streams. In each case a significant interaction effect is present (Top: $p = .001$; Bottom: $p < .001$). Mid line represents data median and the box represents the upper and lower quartiles of the data. Whiskers represent data extremes and data points are indicated on each box plot.

contrast to this pattern, other dorsal stream regions did not demonstrate a double dissociation with the right fusiform gyrus. The right angular gyrus (166–447 ms) and right supramarginal gyrus (279–370) did not show this double dissociation, suggesting that these regions may respond to both Orientation and Identity. However, the right angular gyrus also showed evidence of greater activation to violated expectations about face identity than to violated expectations about head orientation.

Overall, these findings are consistent with our predictions. The left angular gyrus is a dorsal visual stream area that has previously been implicated in visuo-spatial tasks, such as directionality discrimination (Ardila et al., 2000; Hirnstein et al., 2011). In the current study, the left angular gyrus showed a clear double dissociation with the right fusiform gyrus, generating expectation violation signals to unexpected head orientations but not to unexpected face identities. This is consistent with the core idea that prediction-errors about orientation are detected at the level of the processing hierarchy that resolves object orientation. This result is also consistent with our previous research localising prediction-error signals to face and body orientation (Johnston et al., 2017), since the (right) angular gyrus was one of the main regions reported in that study. Indeed, in the present study the right angular gyrus was also identified in the analysis demonstrating a significant early to mid-latency response window and was not doubly-dissociated between Orientation and Identity violations. The right angular gyrus has previously been identified for its critical role in sequence learning (Rosenthal et al., 2009). The left postcentral gyrus also showed a double dissociation with the right fusiform gyrus, however this cluster showed a slightly later evoked response. This may represent a higher-level response to violated expectation, as postcentral regions have previously been implicated in the perception of head and face Orientation (Pageler et al., 2003; Watson and De Gelder, 2016).

A number of cortical areas showed evidence of greater early to mid-latency violations to Violated Identity than to Violated Orientation. Our findings in the FG are consistent with fMRI adaptation data demonstrating a reduction in responses after repeated face identities (Andrews and Ewbank, 2004), not present when time variant aspects of faces were changed. Our findings are also consistent with work by Simpson et al. (2015) showing adaptation effects to repeated identities in the FG despite not inducing strong identity expectations. The results are also consistent with our previous findings (Johnston et al., 2016) indicating greater response in early latencies to rare as compared to frequent

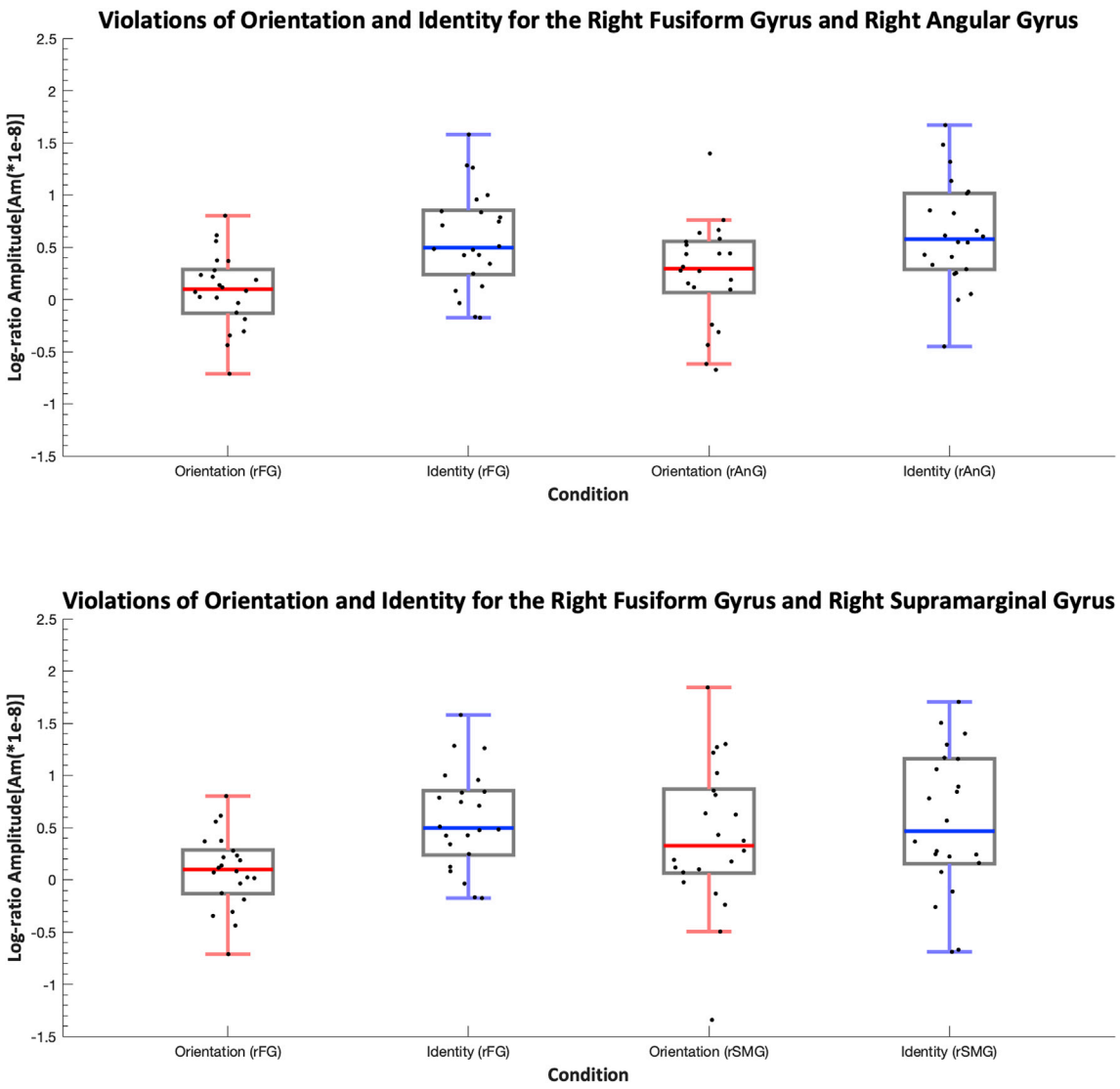

Fig. 7. Difference box plots of Identity (in blue) and Orientation (in red) condition for the log-ratio (Violated/Non-violated) of average amplitude across selected windows (see Table 3). The plots show pairs of regions from the ventral and dorsal streams. In the top graph a significant main effect of Expectation Type is present ($p < .001$). Mid line represents data median and the box represents the upper and lower quartiles of the data. Whiskers represent data extremes and data points are indicated on each box plot.

identities in ambient image sequences. A right lateralisation of this response, as in the present study, is not uncommon following the presentation of face stimuli (Kanwisher et al., 1997; Morris et al., 2007).

As with all MEG source localisation analyses, it should be noted that the beamformer gives an estimate of sources within the brain. However, so consistent was our localisation of the FG with that of fMRI studies of facial identity (Andrews and Ewbank, 2004), that we are confident in the veracity of the metric used here for source localisation.

The right supramarginal gyrus showed mid-latency expectation violation signals in response to unexpected Orientation and unexpected Identity. It may be that the activity in these areas reflects general responses relating to the reallocation of attention. In our previous work investigating violated expectation for object orientation and identity (Johnston et al., 2016, 2017; Simpson et al., 2015), in addition to early-latency prediction-error signals, we have also consistently identified a later latency peak for violated expectations. Previously we proposed that these components may be related to attentional processes. Most notably, in experiment three of Johnston et al. (2017), where stimuli moved position around the fixation at compass winds, a mid-latency component (N300) was identified that could not be accounted for by the size of the N170. By comparison, in all of our other experiments this late component was proportional to the N170. The fundamental difference being that in experiment three of Johnston et al. (2017) the stimulus changed physical location, suggesting that this mid-latency component is strongly modulated by the reallocation of attention. Indeed, the supramarginal gyrus is commonly implicated in spatial attention (Loayza et al., 2011; Silk et al., 2010). The time window identified at the right supramarginal gyrus also started at latencies consistent with experiment three of Johnston et al. (2017).

The identification of opercular cortex VEs to face identity violations is perhaps surprising, as the opercular cortices are not within the ventral stream. However, Johnston et al. (2017) also previously reported regions in right parietal opercular cortex and right central opercular cortex to violations of expectation for face and body orientation. In the present study we identified greater prediction-error signals to identity violations than to predictable identities in these VEs. These results might initially seem at odds with our previously reported results, but a careful examination of the data suggests otherwise (Supplementary Fig. 3). The current data suggest that differences between Violated and Non-violated orientation and identity are both present, although that the magnitude of violation is much larger to identity. Based on our previous work (Robinson et al., 2018) demonstrating the dose dependency of

prediction-error signals, it may be that violations of person identity simply result in a larger overall prediction-error. Nevertheless, the current study clearly demonstrates prediction-error signalling to violated expectations in both head orientation and face identity. Importantly, these data cannot be attributed to low-level differences between stimuli, because the final sequence transition for trials in each expectation type (across which all comparisons were performed) was identically matched across Violated and Non-violated conditions. Therefore, any condition-specific effects after the onset of the final stimulus must be the result of prior expectations created across the preceding image sequence.

The present study identified a double dissociation of function between a ventral region, the FG, which responds to violation in identity but not orientation and a dorsal region, and the left angular gyrus, which is sensitive to violation in orientation but not identity. The time window identified for each of these VEs began at similar early latencies, suggesting a common process for the perception of violations across different types of expectation within the perception of faces. Thus, we have shown for the first time that prediction-error signals related to specific attributes (identity and orientation) of the same visual stimulus (the face) are localised to distinct cortical regions. These findings are consistent with the idea that the generation of prediction-error signals occurs where the visual feature is processed (Friston, 2005) and that such signals are not widely propagated throughout the visual system.

In general, it seems that the error (violation) signal reflects a combination of the presence and magnitude of the descending prediction and the ascending feature likelihood. In the present study, we followed the suggestion of Trapp et al. (2018) of exploiting the synergy between predictive coding models and theoretical accounts of face perception to show that prediction-error signals to different attributes of a well-studied type of stimulus category, the face, are generated in distinct cortical regions. Although we have used faces as a model stimulus for establishing this finding, the phenomenon is likely to have broad implications and to generalise to different types of stimuli and stimulus attributes, across different sensory modalities.

Ethics statement

Participants were recruited from staff and students at Swinburne University of Technology (SUT), all of whom provided informed consent to participate. The study was approved by the Human Research Ethics Committee of SUT and ratified by Queensland University of Technology's University Human Research Ethics Committee.

Data and Code Availability Statement: Data and code will be made available upon request to the corresponding author: jonathan.robinson@monash.edu.

Acknowledgements

The authors acknowledge the facilities, scientific, and technical assistance of the National Imaging Facility, a National Collaborative Research Infrastructure Strategy (NCRIS) capability, at Swinburne Neuroimaging, Swinburne University of Technology. We also gratefully acknowledge the gentle encouragement of the Oily Rag Foundation (EN10005). We'd also like to thank Jessica Guy, Deborah Loats and the rest of the SUT Babylab team for their involvement in data collection.

Appendix A. Supplementary data

Supplementary data to this article can be found online at https://doi.org/10.1016/j.neuroimage.2019.116325.

References

Allison, T., Puce, A., McCarthy, G., 2000. Social perception from visual cues: role of the STS region. Trends Cogn. Sci. 4, 267–278.
Andrews, T.J., Ewbank, M.P., 2004. Distinct representations for facial identity and changeable aspects of faces in the human temporal lobe. Neuroimage 23, 905–913.
Ardila, A., Concha, M., Rosselli, M., 2000. Angular gyrus syndrome revisited: acalculia, finger agnosia, right-left disorientation and semantic aphasia. Aphasiology 14, 743–754.
Avants, B.B., Tustison, N., Song, G., 2009. Advanced normalization tools (ANTS). Insight J. 2, 1–35.
Baseler, H.A., Harris, R.J., Young, A.W., Andrews, T.J., 2012. Neural responses to expression and gaze in the posterior superior temporal sulcus interact with facial identity. Cerebr. Cortex 24, 737–744.
Bruce, V., Young, A.W., 2012. Face Perception. Psychology Press, Hove, East Sussex.
Carlin, J.D., Rowe, J.B., Kriegeskorte, N., Thompson, R., Calder, A.J., 2011. Direction-sensitive codes for observed head turns in human superior temporal sulcus. Cerebr. Cortex 22, 735–744.
Chen, Y.-S., Cheng, C.-Y., Hsieh, J.-C., Chen, L.-F., 2006. Maximum contrast beamformer for electromagnetic mapping of brain activity. IEEE (Inst. Electr. Electron. Eng.) Trans. Biomed. Eng. 53, 1765–1774.
Dayan, P., Hinton, G.E., Neal, R.M., Zemel, R.S., 1995. The helmholtz machine. Neural Comput. 7, 889–904.
Desikan, R.S., Ségonne, F., Fischl, B., Quinn, B.T., Dickerson, B.C., Blacker, D., Buckner, R.L., Dale, A.M., Maguire, R.P., Hyman, B.T., 2006. An automated labeling system for subdividing the human cerebral cortex on MRI scans into gyral based regions of interest. Neuroimage 31, 968–980.
Eimer, M., 2011. The face-sensitive N170 component of the event-related brain potential. In: Calder, A., Rhodes, G., Johnson, M., Haxby, J. (Eds.), The Oxford Handbook of Face Perception. Oxford University Press, Oxford, UK, pp. 329–344.
Fischl, B., Salat, D.H., Busa, E., Albert, M., Dieterich, M., Haselgrove, C., Van Der Kouwe, A., Killiany, R., Kennedy, D., Klaveness, S., 2002. Whole brain segmentation: automated labeling of neuroanatomical structures in the human brain. Neuron 33, 341–355.
Frazier, J.A., Chiu, S., Breeze, J.L., Makris, N., Lange, N., Kennedy, D.N., Herbert, M.R., Bent, E.K., Koneru, V.K., Dieterich, M.E., 2005. Structural brain magnetic resonance imaging of limbic and thalamic volumes in pediatric bipolar disorder. Am. J. Psychiatry 162, 1256–1265.
Friston, K., 2005. A theory of cortical responses. Philos. Trans. R. Soc. Biol. Sci. 360, 815–836.
Friston, K., Kiebel, S., 2009. Predictive coding under the free-energy principle. Philos. Trans. R. Soc. Biol. Sci. 364, 1211–1221.
Goldstein, J.M., Seidman, L.J., Makris, N., Ahern, T., O'Brien, L.M., Caviness Jr., V.S., Kennedy, D.N., Faraone, S.V., Tsuang, M.T., 2007. Hypothalamic abnormalities in schizophrenia: sex effects and genetic vulnerability. Biol. Psychiatry 61, 935–945.
Grill-Spector, K., Knouf, N., Kanwisher, N., 2004. The fusiform face area subserves face perception, not generic within-category identification. Nat. Neurosci. 7, 555.
Haxby, J.V., Hoffman, E.A., Gobbini, M.I., 2000. The distributed human neural system for face perception. Trends Cogn. Sci. 4, 223–233.
Hirnstein, M., Bayer, U., Ellison, A., Hausmann, M., 2011. TMS over the left angular gyrus impairs the ability to discriminate left from right. Neuropsychologia 49, 29–33.
Hohwy, J., 2013. The Predictive Mind. Oxford University Press, Oxford, UK.
Jenkins, R., Beaver, J.D., Calder, A.J., 2006. I thought you were looking at me: direction-specific aftereffects in gaze perception. Psychol. Sci. 17, 506–513.
Johnston, P., Overell, A., Kaufman, J., Robinson, J., Young, A.W., 2016. Expectations about person identity modulate the face-sensitive N170. Cortex 85, 54–64.
Johnston, P., Robinson, J., Kokkinakis, A., Ridgeway, S., Simpson, M., Johnson, S., Kaufman, J., Young, A.W., 2017. Temporal and spatial localization of prediction-error signals in the visual brain. Biol. Psychol. 125, 45–57.
Kanwisher, N., McDermott, J., Chun, M.M., 1997. The fusiform face area: a module in human extrastriate cortex specialized for face perception. J. Neurosci. 17, 4302–4311.
Kozinska, D., Carducci, F., Nowinski, K., 2001. Automatic alignment of EEG/MEG and MRI data sets. Clin. Neurophysiol. 112, 1553–1561.
Loayza, F.R., Fernández-Seara, M.A., Aznárez-Sanado, M., Pastor, M.A., 2011. Right parietal dominance in spatial egocentric discrimination. Neuroimage 55, 635–643.
Makris, N., Goldstein, J.M., Kennedy, D., Hodge, S.M., Caviness, V.S., Faraone, S.V., Tsuang, M.T., Seidman, L.J., 2006. Decreased volume of left and total anterior insular lobule in schizophrenia. Schizophr. Res. 83, 155–171.
Milner, A.D., Goodale, M.A., 1998. The visual brain in action. Psyche 4, 12.
Mishkin, M., Ungerleider, L.G., Macko, K.A., 1983. Object vision and spatial vision: two cortical pathways. Trends Neurosci. 6, 414–417.
Morris, J.P., Pelphrey, K.A., McCarthy, G., 2007. Face processing without awareness in the right fusiform gyrus. Neuropsychologia 45, 3087–3091.
Nichols, T.E., Holmes, A.P., 2002. Nonparametric permutation tests for functional neuroimaging: a primer with examples. Hum. Brain Mapp. 15, 1–25.
O'Toole, A.J., Roark, D.A., Abdi, H., 2002. Recognizing moving faces: a psychological and neural synthesis. Trends Cogn. Sci. 6, 261–266.
Pageler, N.M., Menon, V., Merin, N.M., Eliez, S., Brown, W.E., Reissa, A.L., 2003. Effect of head orientation on gaze processing in fusiform gyrus and superior temporal sulcus. Neuroimage 20, 318–329.
Peirce, J.W., 2007. PsychoPy—psychophysics software in Python. J. Neurosci. Methods 162, 8–13.
Peirce, J.W., 2009. Generating stimuli for neuroscience using PsychoPy. Front. Neuroinf. 2, 10.
Robinson, J.E., Breakspear, M., Young, A.W., Johnston, P.J., 2018. Dose dependent modulation of the visually evoked N1/N170 by perceptual surprise: a clear demonstration of prediction-error signalling. Eur. J. Neurosci. 1–11. https://doi.org/10.1111/ejn.13920.
Rosenthal, C.R., Roche-Kelly, E.E., Husain, M., Kennard, C., 2009. Response-dependent contributions of human primary motor cortex and angular gyrus to manual and perceptual sequence learning. J. Neurosci. 29, 15115–15125.

Silk, T.J., Bellgrove, M.A., Wrafter, P., Mattingley, J.B., Cunnington, R., 2010. Spatial working memory and spatial attention rely on common neural processes in the intraparietal sulcus. Neuroimage 53, 718–724.
Simpson, M.I., Johnson, S.R., Prendergast, G., Kokkinakis, A.V., Johnson, E., Green, G.G., Johnston, P.J., 2015. MEG adaptation resolves the spatiotemporal characteristics of face-sensitive brain responses. J. Neurosci. 35, 15088–15096.
Trapp, S., Schweinberger, S.R., Hayward, W.G., Kovács, G., 2018. Integrating predictive frameworks and cognitive models of face perception. Psychon. Bull. Rev. 1–8.
Watson, R., De Gelder, B., 2016. The neural basis of individual face and object perception. Front. Hum. Neurosci. 10, 66.
Young, A.W., 2018. Faces, people and the brain: the 45th sir frederic bartlett lecture. Q. J. Exp. Psychol. 71, 569–594.
Yushkevich, P.A., Piven, J., Hazlett, H.C., Smith, R.G., Ho, S., Gee, J.C., Gerig, G., 2006. User-guided 3D active contour segmentation of anatomical structures: significantly improved efficiency and reliability. Neuroimage 31, 1116–1128.